Low-carbon Fuels for Spark-ignited Engines: A Comparative Study of Compressed Natural Gas and Liquefied Petroleum Gas on a CFR Engine with Exhaust Gas Recirculation

Toluwalase Fosudo[a], Tanmay Kar[a], Bret Windom[a], Daniel Olsen[a]

[a]*Department of Mechanical Engineering, Colorado State University, 1374 Campus Delivery, Fort Collins, 80523-1374, Colorado, USA*

Abstract

Decades of work on low-carbon fuels have established their potential for substantial emissions reductions; however, their adoption is still limited by infrastructure concerns and engine efficiency deficits. As infrastructures have begun to evolve, research on strategies that maximize engine efficiency through interactions with fuel properties must also now take center place. This paper compares the performance, emissions, and combustion characteristics of two forefront low-carbon fuels: compressed natural gas (CNG) and liquefied petroleum gas (LPG) in a cooperative fuel research (CFR) engine over a range of compression ratios and engine loads. The effects of exhaust gas recirculation (EGR), end-gas auto-ignition, and a novel combustion control tool, the combustion intensity metric (CIM), were also evaluated at different stoichiometric engine operating conditions. In comparison to LPG, CNG operation demonstrated an extended knock-free regime, allowing engine operation at higher engine loads and compression ratios, but LPG operation

exhibited enhanced combustion characteristics with higher peak pressures and faster apparent heat release rates (AHRR). LPG operation achieved higher brake thermal efficiencies and lower equivalent CO_2 emissions compared to CNG operation at the tested engine loads and compression ratios. LPG demonstrated significantly higher EGR tolerance limits compared to CNG, with a maximum of 28% EGR rate, compared to 23% for CNG. This improved EGR dilution tolerance was responsible for a 90% reduction in NOx emissions for LPG compared to a maximum of 70% with CNG. EGR dilution also exhibited more effective knock mitigation potential with LPG, suppressing knock intensity values by up to 98% and transitioning the engine operation towards normal combustion from heavy knocking conditions. The CIM was found to decrease burn durations and improve the quality of combustion by controlling the desired fraction of end-gas auto-ignition.

Keywords: Liquefied petroleum gas, Compressed natural gas, Exhaust gas recirculation, Spark-ignited engines, End-gas auto-ignition, Brake specific emissions

1. Introduction

It is undeniable that fossil fuels have moved our world forward for over a century and are still doing so. In 2021, the primary energy source in the U.S. transportation sector at over 94% was fossil fuels, contributing about 25 quadrillion BTU [1]. However, this forward momentum has been continually blighted by inefficiencies in the use of these fuels and the adverse effect of their

emissions on the environment. Globally, the transportation sector is responsible for 37% of the carbon dioxide (CO_2) emissions from end-use sectors [2], accounts for over 20% of energy consumed, and contributes 14% to greenhouse gas emissions [2 - 4]. In a concerted effort to remedy this situation, research on cleaner alternative fuels development and adoption has gained prominence in the last few decades [5 - 8]. However, significant re-engineering of the current, well-established fuel handling, transportation, and storage infrastructures may be required before alternative fuels can significantly contribute to end-use energy consumed [9, 10]. Therefore, viable short to middle-term alternative fuel options should aim to utilize existing infrastructure. In tandem, these fuels should exhibit a potential for lower engine-out emissions, and higher or comparable efficiencies with conventional fuels used in spark ignition (gasoline) or compression ignition engines (diesel). In spark ignition (SI) engines, the focus for alternative fuel development is increasing efficiency [4, 5, 11] and extending the knock limit [5]. Knock is an undesirable abnormal combustion phenomenon [12] where the end-gas ahead of the flame front auto-ignites sporadically, causing a rapid pressure rise and ‘ringing’ sound in the combustion chamber. Typically, octane numbers (ON) have been used as a measure of resistance to knock for liquid fuels and methane numbers (MN) for gaseous fuels [13 - 15]. The higher the ON, the more resistant the fuel may be to knock, permitting an increase in compression ratio and, consequently, in efficiency [11, 13]. Therefore, possessing an ON higher than gasoline is a desirable attribute of

viable alternative fuels for SI engines.

Two such promising alternative, low-carbon fuels are natural gas and liquefied petroleum gas (LPG). Natural gas, composed predominantly of methane, is obtained from underground reservoirs and is stored either as compressed natural gas (CNG) or liquefied natural gas (LNG) [8]. Similarly, LPG is composed mainly of propane and n-butane [16] and is refined from crude-oil or is obtained as a by-product from the processing of natural gas [8]. Previous studies conducted with CNG and LPG engine fueling have spanned different areas of research including dual-fuel applications, fuel injection phase and hardware development, heavy-duty application, effect of fuel composition, end-gas auto-ignition, exhaust gas recirculation etc. Singh et al. [17] investigated the operation of a turbocharged dual-fuel engine with natural gas and gasoline. Their results indicated a decrease in CO_2 emissions as engine load was increased but nearly 20% more CO_2-equivalent emissions as a result of higher methane emissions [17]. Investigations by Nutu et al. [18] with LPG indicated a 20% reduction in brake specific energetic consumption and 25% lower oxides of nitrogen for an LPG substitution ratio of 25 in a dual fuel engine [18]. Studies on the effect of NG and LPG composition on dual fuel and single fuel SI engine operation indicate a significant effect on knocking behaviors and engine-out emissions. For example, experimental studies conducted by El Najjar et al. [19] on the performance of a dual fuel engine using different LPG blends indicated a relationship between knock, pilot fuel injection timing and LPG

composition [19]. Saleh [20] showed that increasing propane concentration in the LPG blend composition led to reduced CO emissions while higher levels of butane led to lower NOx emissions for a dual fuel diesel engine [20]. Fosudo et al. [15] investigated the effect of variable LPG composition on a premixed SI engine and showed that resistance to knock was linked to the concentration of butane, propylene and ethane present in the LPG blend [15]. Bestel et al. [21] conducted numerical and experimental studies on the mechanics of end-gas auto-ignition for various CNG blends on an SI engine. They found that the auto-ignition duration was influenced by NG composition while the knock onset crank angle was mostly similar for all the blends [21]. Mohr et al. [22] characterized the flame propagation rate and ignition delay for several CNG mixtures with EGR in a rapid compression machine. Their results indicated that the reactive species in the recirculated exhaust gases (CO and NO) and the fuel reactivity had a substantial effect on end-gas auto-ignition fraction [22].

In heavy-duty applications, CNG and LPG have demonstrated significant gains in terms of emissions. Meyer et al. [23] converted a diesel engine to a natural gas engine and reported 2.9g/kW-hr of NOx emissions for the CNG compared to 7.4g/kW-hr for the baseline diesel engine with only a moderate efficiency drop [23]. Likewise, Barroso et al. [24] converted a 13L diesel engine to a lean-burn natural gas engine. They reported a potential for lowering the specific particulate matter (PM) emissions with natural gas fueling, but they recorded lower torque values than the baseline diesel engine at all engine speeds

[24]. Khan and Watson [25] investigated the use of a light duty LPG engine for heavy duty application and showed emissions and efficiency engine maps [25]. Their results indicated an 18% reduction in CO_2 at lambda (λ) 1.4 when compared to the diesel case and approximately equal efficiencies when compared to the gasoline case at the same compression ratio and stoichiometric conditions [25]. There was also an uptick in hydrocarbon emissions as lambda was increased [25]; a similar trend was observed by Fosudo et al. in their heavy-duty LPG engine experiments [26]. As regards fuel delivery, Pradeep et al. [27] compared port-injected and carbureted gaseous LPG on a single cylinder engine and discovered a 22% improvement in BTE with the port-injected case [27]. Darzi et al. [28] studied the effect of port-injected and fumigated natural gas at compression ratios (CR) 14 and 17 on a two-stroke engine. The results showed a decrease in efficiency for both CNG cases compared to the baseline gasoline at CR 14 [28]. As a result of its huge potential, several studies have detailed the development of liquid LPG direct injection (DI) hardware [29 - 32] and showed improvements in BTE and reduction in HC emissions when compared with manifold injection [33, 34]. Dube et al. [33] conducted experimental investigations on a 2-stroke engine with liquid phase DI LPG. The DI operation achieved an 87% reduction in HC emissions and 6.6% absolute improvement in BTE at 70% throttle compared to the manifold injection configuration [33]. Pradeep et al. [34] also reported similar numbers at 100% throttle, demonstrating an 88% reduction in HC emissions and 8% absolute improvement in BTE with

DI LPG compared to manifold injected LPG [34]. For DI CNG, Kalam et al. [35] investigated the performance of a natural gas engine compared with a CNG bi-fuel and baseline gasoline port-injection engine. The results indicated that the DI CNG operation reduced NOx by 42% compared to gasoline port-injection and produced 23% higher brake power than the bi-fuel operation [35]. Numerically, Fan et al. [36] studied the impact of injection angle and timing on combustion and mixture formation in a natural gas DI engine.

Finally, in terms of combustion, there have been several investigations on end-gas auto-ignition, knock, and the effect of exhaust gas recirculation (EGR) on engines fueled with CNG and LPG. Bestel et al. [37] developed a multidimensional model of an SI CNG engine which was capable of predicting pressure rise rate and the onset of end-gas auto-ignition of varying intensities for various engine operating conditions [37]. Bestel et al. [38] also developed a method to detect the occurrence and onset of end-gas auto-ignition in a premixed CNG SI engine using a representative apparent heat release rate curve [38]. Rodriguez et al. [39] converted a 6-cylinder diesel engine to a single cylinder CNG SI engine with EGR and conducted a series of baseline experiments. They reported an optimal BTE of 39.9% at 10% EGR substitution and high load conditions [39]. Ravi et al. [40] investigated the influence of cooled EGR on the performance of a lean-burn LPG SI engine. They reported an inverse relationship between the optimum level of EGR and fuel flow rate [40]. Kar et al. [41, 42] performed numerical and experimental studies on the effect of

EGR and fuel formulation on a premixed LPG SI engine. They demonstrated the rapid consumption of CH_2O and formation of substantial OH species during end-gas auto-ignition [41] and showed the reducing effect of EGR on this chemistry [42]. Krieck et al. [43] studied the preignition and knock behavior of LPG in an SI engine. Their results indicated that high LPG fuel temperature had a deleterious impact on pre-ignition resistance [43]. Investigations by Morganti et al. [44] showed that the NO concentration in the residual gas was a potent promoter of auto-ignition especially when compared to UHCs and CO which both had negligible effects on propane auto-ignition [44]. Hampson et al. [45] differentiated between the destructive knocking combustion and a desirable flame-front initiated volumetric end-gas auto-ignition that speeds up the combustion process [45]. They described the development and application of an advanced combustion control tool, the combustion intensity metric (CIM), which was designed to influence the auto-ignition process during engine operation and control the fraction of end-gas auto-ignition (f-EGAI) to a desired amount [45]. This technique has been successfully applied to natural gas engines showing efficiency and combustion benefits especially with EGR [21, 22, 38, 45 - 50]. For example, Nair et al. [48] achieved faster combustion and reported higher-than-diesel efficiencies on a CIM-controlled dual fuel diesel/CNG engine while Bayliff et al. [49] demonstrated an improvement in BTE as f-EGAI was increased, with a reported maximum BTE at 34% f-EGAI on a CNG engine. In terms of EGR, Bayliff et al. [50] also reported a 28% relative increase in the

BTE and about 66% NOx reduction on a stoichiometric NG engine as EGR was introduced [50]. Splitter et al. [51] reported that LPG combustion allowed higher EGR rates compared to gasoline and found that at high EGR rates and CR with late intake valve closing, DI LPG produced diesel-like power density on a high stroke-to-bore ratio SI engine [51]. Recent studies by Ge et al. [52] showed that this higher EGR tolerance of LPG compared to gasoline was not due only to flame speeds but was also possibly linked to flame structures and the comparatively lower Lewis number of LPG [52]. They concluded that further work comparing the EGR tolerances of LPG and a lower Lewis number fuel like Methane was necessary [52].

The foregoing review reveal that further research is still required especially in the area of conversion efficiency, exhaust gas recirculation, end-gas auto-ignition and the development of advanced combustion strategies before these two low-carbon, alternative fuel options can substantially address the emission burden of conventional fuels. This research is the first phase of a larger project with set goals to develop high efficiency alternative fuel heavy-duty engines. As fleet managers consider several alternative fuel options in their decision-making process, this direct comparison of these two choice fuels provides useful insights and adds to the body of knowledge. This paper first explores the combustion, performance, and emissions behavior of LPG and CNG across different compression ratios and engine loads on an SI cooperative fuel research (CFR) engine. The study then experimentally expands on recent numerical work done

by Ge et al. [52] by comparing the EGR dilution tolerance of the two fuels, CNG and LPG, for a given load and at two compression ratios. The authors have found no articles that have undertaken this investigation that improves the understanding of the interaction of these fuels with EGR. Finally, this paper is the first the authors have found to apply the novel combustion control tool, the combustion intensity metric (CIM) to an LPG engine. The paper extends previous work done exclusively with natural gas engines, by exploring the end-gas auto-ignition behavior and combustion benefit of using the CIM on an SI engine fueled with LPG. In the experimental investigations, pipeline natural gas (86% methane) and locally supplied LPG (95% propane) were used for the performance, emissions, and combustion comparison and the results discussed.

2. Material and methods

The tests in this experimental study were conducted on a single cylinder, 4-stroke cooperative fuel research (CFR) engine. The SI research engine produced by Waukesha Motor Company, was designed as a variable compression ratio engine for defining gasoline fuel quality in a standardized set-up. The test engine specifications are provided in Table 1. Several modifications were made to the original test engine to allow operation on gaseous fuels. This customization included the installation of several measuring instruments at specific locations to obtain accurate measurement of engine operating parameters and results. A detailed description of the measurement devices and methods used in this study is provided below.

Table 1: The test engine specifications

Model	Waukesha CFR F-1/F-2
Displacement volume	611.7cc
Bore x Stroke	82.55mm x 114.3mm
Connecting rod	254mm
Compression ratio	4:1 - 18:1, Adjustable
Number of cylinders	1
Cylinder type	Flat combustion surface, cast iron
IVO and IVC	10°aTDC and 146°bTDC
EVO and EVC	140°aTDC and 15°aTDC
Number of valves	2

A Yaskawa U1000 regenerative variable frequency drive was installed to ensure accurate speed control. The industrial MATRIX drive is capable of maintaining speeds between 600 and 1200RPM. All the tests in this study were performed at 900RPM engine speed. A BEI model L25 incremental optical encoder was also installed on the crankshaft to provide crank angle position with a tenth of a degree resolution. Three Kistler high-speed pressure transducers were used in this study; a 6061B water-cooled piezoelectric transducer provided in-cylinder pressure readings, while dynamic intake and exhaust pressure measurements were made with the 4007D and 4049B piezoresistive transducers respectively. Several absolute pressure transducers from Omega Engineering and K-type thermocouples were installed at strategic locations to measure pressure and temperature of the fuel, oil, coolant, and intake and exhaust buffer volumes at all engine operating conditions. To maintain a constant vapor

pressure inside the LPG cylinder irrespective of fluctuations in the ambient conditions, a heated blanket was wrapped around the tank and an electrically heated Swagelok K-series pressure regulator and heat trace were introduced on the fuel delivery line to preserve the fuel supplied to the engine in the gas phase. A Micromotion CMF series Coriolis mass flow meter downstream of the heated regulator was used to measure the flow rate of the fuel while a wide-band LSU 4.9 lambda sensor with operating range lambda (λ) 0.65 to ∞ and exhaust temperatures up to 930°C located downstream of the exhaust buffer volume provided a measure of the air-fuel ratio in the engine. In this work, exhaust gases were continuously sampled from the exhaust buffer volume through a heated line connected to a Fourier transforms infrared (FTIR) spectrometer from MKS Instruments. The FTIR spectrometer provided measurements of CO_2, CO, NOx, and THC, as well as other compounds of interest, for example, non-methane hydrocarbons (NMHC). A detailed description of the FTIR system can be found in the research work done by Fosudo et al. [15].

The brake thermal efficiency was calculated using equation 1, where an NK APT-TH series 10kW power transducer was used to measure the electrical output from an induction motor connected to the engine. Note that the efficiency of the induction motor in the generator mode is known from the manufacturer's specification sheet.

$$\eta_b = \frac{(\dot{W}_e/\eta_{gen})}{\dot{m}_f * LHV} \quad (1)$$

where η_b is the brake thermal efficiency (%), $\dot{W}_e$ is the electrical power output (kW), η_{gen} is the generator efficiency and $\dot{m}_f$ is the fuel mass flow rate (g/s).

A time-averaged technique was applied to quantify knock in this work. Previous studies have described this method in detail [50, 53]. The knock quantification method involved applying a bandpass filter and then a fast Fourier transform (FFT) to the measured in-cylinder pressure. The FFT power spectrum amplitudes were recorded for every engine cycle and integrated over a set number of cycles to obtain a knock integral (KI). This integral, shown in equation 2, provided a consistent and objective metric for the comparison of knock intensities at all tested engine operating conditions.

$$KI = KL(1) + KL(2) + KL(3) + \cdots + KL(n) \tag{2}$$

where KI is the knock integral, KL is the knock amplitude for each individual cycle, and n is the number of consecutive cycles integrated over, taken as 200 in this paper.

The apparent heat release rate (AHRR) was calculated from the measured in-cylinder pressures using equation 3 which is derived based on the first law single zone model [12].

$$\frac{dQ}{d\theta} = \frac{\gamma}{\gamma - 1} P \frac{dV}{d\theta} + \frac{1}{\gamma - 1} V \frac{dP}{d\theta} \tag{3}$$

where Q is the heat release, γ is the polytropic constant taken as 1.35, P is the in-cylinder pressure, and V is the cylinder volume.

The combustion control system from Woodward Inc. was used to monitor the effects of several key combustion metrics in real-time so as to detect and control end-gas auto-ignition (EGAI) to a desired fraction [48]. This desired EGAI fraction, f-EGAI, is defined as the fraction of chemical energy release that occurs after the onset of end-gas auto-ignition has been detected. This f-EGAI was reliably controlled using a parameter called the combustion intensity metric (CIM) which is a linearly scaled combination of the variables shown in equation 4 with respect to their reference values.

$$CIM = A_1 \frac{P_{max}}{P_{max_{ref}}} + A_2 \frac{BD}{BD_{ref}} + A_3 \frac{PRR}{PRR_{ref}} + A_4 \frac{HRR_S}{HRR_{S_{ref}}} + A_5 \frac{KI}{KI_{ref}} \quad (4)$$

where A_x are calibration constants, Pmax is the peak pressure (bar), BD is the burn duration (CAD), PRR is the pressure rise rate (bar/deg), HRRs is the heat release rise rate slope (J/deg/deg), and KI is the knock intensity. The CIM is a sophisticated combustion control tool that analyzes and incorporates the knock intensity, heat release, and pressure trends on a real-time, cycle-to-cycle basis, detects the onset of end-gas auto-ignition and essentially adjusts combustion phasing to output the required f-EGAI value. This combustion mode is defined as controlled end-gas auto-ignition (c-EGAI) which offers a more robust engine operation, as it, incorporates other conventional methods of setting the spark

timing like knock intensity in its consideration and has been shown to shorten combustion duration especially in dilute (lean and EGR) engine operation [48, 49]. It also monitors several key combustion trends in real-time and as such can allow engines respond quicker to transient operation in practical situations and operate closer to their limits without engine damage. The CIM which is an embedded parameter in the Woodward engine control module used in this study was calibrated for each fuel-specific engine operation.

Exhaust gases were extracted after the exhaust pressure transducer location, cooled by a water-cooled heat exchanger, and then recirculated back into the intake system. The EGR rate was calculated using equation 5.

$$EGR\% = \frac{\dot{m}_{EGR}}{\dot{m}_{EGR} + \dot{m}_{air} + \dot{m}_{fuel}} \tag{5}$$

where $\dot{m}_{EGR}$, $\dot{m}_{air}$, and $\dot{m}_{fuel}$ are the measured mass flow rates (g/s) of the recirculated exhaust gases, air, and fuel, respectively.

Finally, nominal repeat tests were conducted for every day of testing at the same engine operating condition to determine the random uncertainty with the assumption that system uncertainties remained constant on the unchanged test cell. The random uncertainty for each measured variable was then propagated to the results of interest using the root of summation of squares equation [54] in equation 6.

$$\omega_R = (\sum_{i=1}^{n} [\omega_{x_i} \frac{\delta R}{\delta x_i}]^2)^{1/2} \quad (6)$$

where ω_{x_i} are the uncertainties in the variables x_i, and ω_R is the uncertainty in the result R.

The test cell is shown in Figure 1 and a schematic diagram can be found in [15].

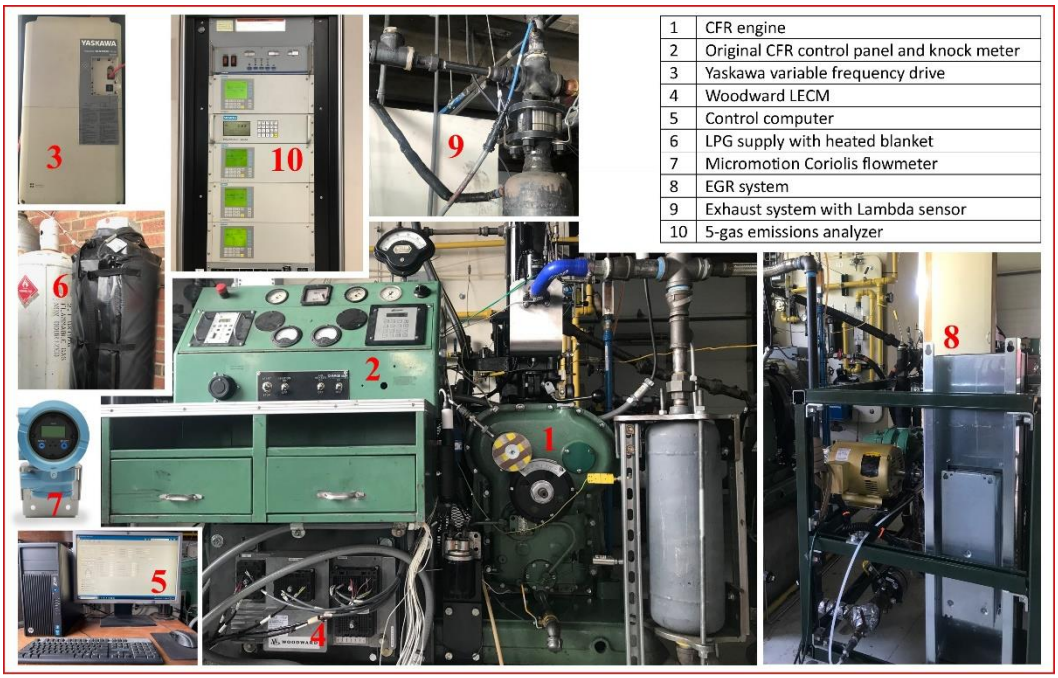

Figure 1: The CFR test cell

3. Test Procedure

The experiments, in Table 2, were designed to study the performance of the two low-carbon fuels, LPG and CNG, on the CFR engine. All tests were conducted at stoichiometric, naturally aspirated conditions and with a

combustion phasing of CA50 9.5°aTDC except as otherwise required. First, compression ratio (CR) was swept from a non-knocking engine operating condition, 7:1, to knocking conditions for both fuels. Subsequently, engine load represented by the net indicated mean effective pressure (IMEP) was swept from 8bar to the load limit of the engine at 11bar by increasing the intake air manifold pressure (IMAP). EGR was then added to the intake charge in 5% increments at CR 8:1 and 10% increments at CR 9:1 and at a constant, high engine load of 10bar until the EGR limit, described by an unsteady operation of the engine was reached. Combustion phasing control was then switched from CA50 to CIM, which was swept in 10% increments until the occurrence of heavy knock at high loads, for a baseline CR and with IMAP kept constant. This baseline CR was found by increasing the CR on the CFR engine at naturally aspirated conditions until the onset of incipient knock and then reducing the CR gently until there was no knock.

Table 2: Experimental test matrix

Parameter	LPG	Natural Gas
Compression Ratio (CR)	7 - 10	7 - 10, 12
Engine Load (bar)	8 - 11	8 - 11
$EGR_{@CR8}$ (%)	10 - 30	10 - 25
$EGR_{@CR9}$ (%)	10 - 30, 35	10 - 30
CIM (%)	0 - 80	0 - 80
Engine operating conditions: ϕ = 1, Speed = 900RPM, Coolant Temp. = 95°C, Oil Temp. = 55-60°C, Mixture Temp. = 60°C IMAP = 1.013bar, CA50 = 9.5°aTDC***		

In-cylinder pressure data was managed using a high-speed National Instruments PCI 6251 data acquisition card, while a combination of the Woodward Large Engine Control Module (LECM) and LabView were used for real-time control and monitoring of the CFR. The LECM performed real- time analysis of this in-cylinder pressure to achieve the desired combustion phasing and combustion data was logged on the LECM for 200 cycles. High-speed in-cylinder and manifold pressures were logged on LabView for 1000 consecutive cycles. Other parameters of import such as flowrates, electric power, lambda (λ), and temperatures were monitored and recorded for 3 minutes on LabView. All engine data was recorded at steady engine operation defined by a COV_{IMEP} below 3%.

In this study, pipeline natural gas supplied to the research facility was used for the CNG tests. LPG with constituents conforming to the U.S. HD-5 standard was specified and certified by a local gas supplier to a +/-2% accuracy. Fuel samples were collected and also constantly monitored during engine operation using an INFICON Micro GC to ensure constancy of fuel composition and provide gas chromatography results. The properties and composition of the fuels are shown in Table 3.

Table 3: Test fuel properties [55, 56, 57]

Composition (% vol)	**LPG**	**Natural Gas**
Methane	-	86.01
Ethane	0.01	10.05
Propane	95.64	1.34
Propylene	2.53	-
n-Butane	1.75	0.15
i-Butane	0.05	0.09
n-Pentane	-	0.02
i-Pentane	-	0.02
Nitrogen	0.02	0.36
Carbon dioxide	-	1.96
Properties		
LHV (MJ/kg)	46.32	46.8
Laminar flame speed (cm/s)	40.32	36.65
Stoichiometric AFR	15.54	15.98
H:C ratio	2.65	3.69
Methane Number	33	74
Autoignition temperature (°C)	454 - 510	540

4. Results and Discussion

This study presents a comparison of the combustion, emission, and performance characteristics of two select low-carbon fuels: LPG and CNG, on a single cylinder CFR engine. Combustion parameters such as in-cylinder pressures and AHRR were analyzed, engine-out emissions like NOx were evaluated in a brake power normalized format, and performance was quantified in terms of brake thermal efficiencies (BTE). The investigations were performed at different compression ratios, engine loads, EGR rates, and CIM% for each fuel and the following results obtained.

4.1. Effect of Compression Ratio

This section discusses the effect of compression ratio on the characteristics of both fuels. First, Figure 2a presents a measure of the knock intensity as CR was increased from a non-knocking CR of 7:1 for both fuels. A subjective limit above which knock began to occur on the CFR engine was defined as KI = $6kPa^2$. As CR was increased to 8:1, LPG began to experience incipient knock, developing rapidly to medium knock at CR 9:1 and on to heavy, destructive knock at 10:1. Meanwhile, CNG did not experience any form of knock until CR 10:1 while also demonstrating a gentler rise, compared to LPG, to medium knock which was induced at CR 12:1. This variation in knocking tendency is due to the composition of both fuels. The longer carbon chains in the dominant component of the LPG, Propane, has a higher knocking tendency than that of the primary component of the CNG, Methane [12]. This difference can be

quantified in terms of octane numbers (ON), where the higher ON for CNG (120) enables it to be more resistant to knock than LPG (104) [8, 9]. Also, since they were both introduced as gaseous fuels on the test cell, a comparison of methane number (MN) shown in Table 3 supports the higher knocking tendency of LPG over CNG. Results from Malenshek et al. [14] showed that fuels with similar MN to the LPG and CNG fuels used in this study experienced knock at approximately the same CR as those observed in the present study.

Next, the in-cylinder pressure traces and AHRR at CR 7:1, 10:1 and 12:1 (CNG only) are shown as a function of CR in Figure 2b. LPG combustion indicated a higher AHRR at all conditions with a shorter duration of heat release compared to CNG which translates to quicker fuel energy release and shorter combustion durations in favor of LPG. In terms of the in-cylinder pressures, LPG indicated peak pressures higher by 6% at CR 7:1 and then by 22% at CR 10:1 compared to CNG and also exhibited more advanced location of peak pressures (LPP) at both CR. However, it is desirable to increase CR, peak pressures, and advance LPP without the occurrence of destructive knock and CNG achieved the highest CR (i.e., CR 12:1) and peak pressures recorded during the CR tests with only medium knock. The steeper slope after the inflection point on the LPG pressure trace at CR 10:1 even compared to CNG at CR 12:1 indicated a rapid rate of pressure rise typically associated with end-gas auto-ignition.

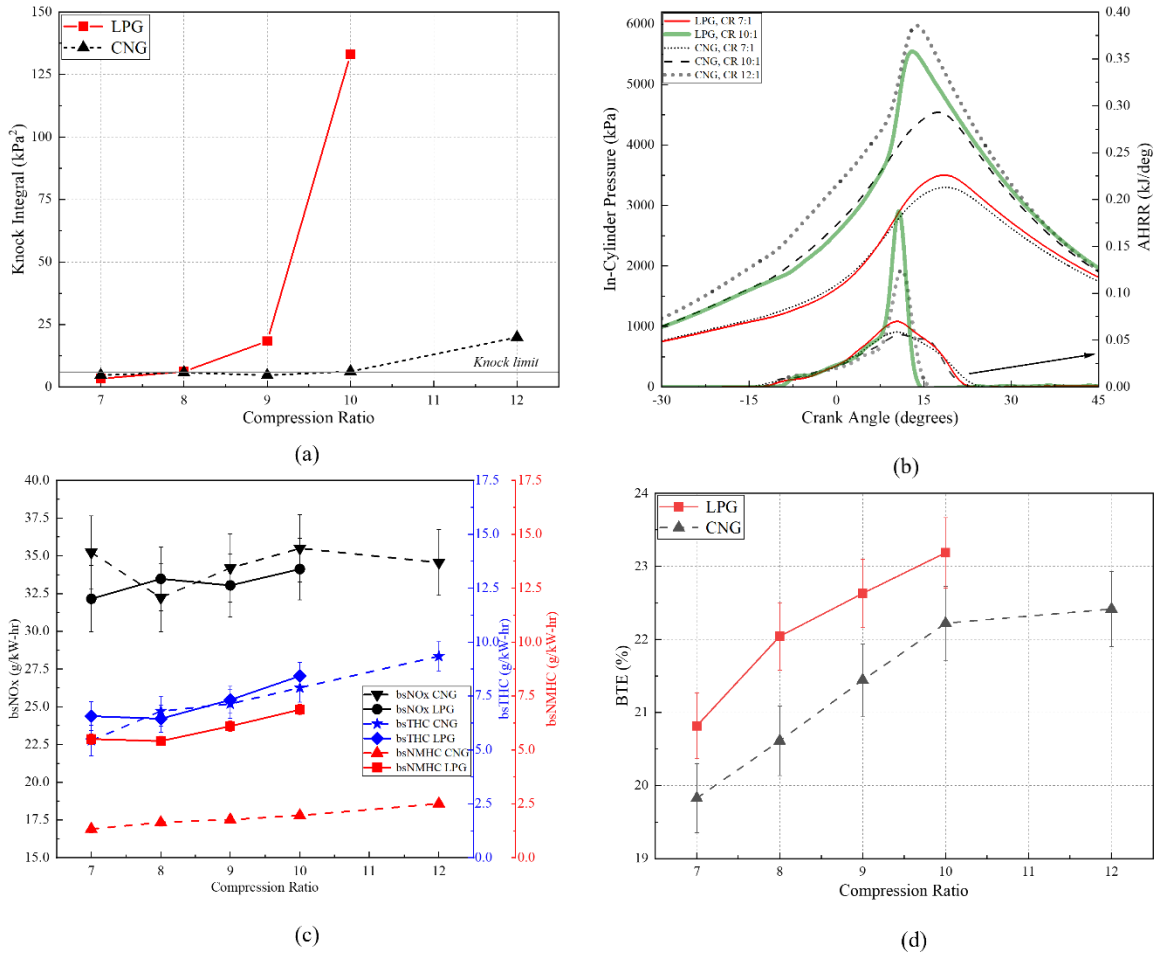

Figure 2: Variation of (a) Knock Integral (b) In-cylinder pressure and AHRR (c) brake specific emissions (d) BTE, with compression ratio for CNG and LPG

In addition, the brake specific (bs) NOx, THC and NMHC are graphed in Figure 2c. The exhaust sampling results showed that LPG produced slightly higher ppms of NOx compared to CNG; for example, at CR 9:1 LPG NOx emissions were recorded as 4078ppm compared to 3941ppm for CNG at the same CR. However, this trend was reversed upon normalization with brake power as presented in Figure 2c, as a result of the higher brake powers generated

by LPG at every CR. Since NOx chemistry is primarily determined by local in-cylinder temperatures, an approximation for the peak in-cylinder temperatures was determined using the ideal gas equation and this showed higher peak temperatures for LPG across all CR which supports the higher NOx ppm values for LPG. In terms of the CR effect alone, as CR increases, pressure and temperature also increase with a consequent increase in NOx ppm observed in this study. However, this increasing effect was counteracted by the reducing effect of the normalization with higher brake powers at higher CR. The bsTHC emissions in Figure 2c described a more distinctive increasing trend with CR. This is likely largely due to the crevice volume effect, with the high in-cylinder pressures recorded at high CR forcing more gas into the crevices. This gas then rejoins the exhaust stream during the expansion stroke as unburned hydrocarbons (UHC).

Comparing both fuels, LPG indicated higher bsTHC than CNG except at CR 8:1, with the most being 8.4g/kW-hr at CR 10:1, 7% more than the bsTHC of CNG at this CR. Another important class of regulated emissions for SI LPG engines are NMHC, as such the bsNMHC emissions were also evaluated and plotted in Figure 2c. CNG operation reduced bsNMHC emissions compared to LPG by over half at every tested CR showing an almost 72% reduction at CR 10:1. This reduction was due to the composition of the CNG (i.e., 86% CH_4 by vol) and the fact that a larger percentage of its THC emission was made up of CH_4. However, CH_4 is a potent contributor to GHG and should also be

minimized. The notable difference in Figure 2c between the bsTHC and the bsNMHC numbers is the bsCH_4, which increases with CR as observed from the divergence between the bsTHC and bsNMHC lines. This divergence is likely due to the greater rate of low temperature oxidation of higher hydrocarbons on reentry into the combustion chamber from the crevice volume compared to CH_4. Similar NMHC/CH_4 behavior of LPG and CNG has also been reported in the literature [58].

Finally, the performance metrics are presented in terms of BTE in Figure 2d, where BTE was observed to increase in tandem with CR due to improved cycle efficiency [12, 15]. LPG indicated a higher BTE value at every tested CR when compared with CNG, with a maximum relative increase of 7% at CR 8:1, where LPG had an efficiency of 21.54% compared to 20.11% with CNG fueling. This can be attributed to the combined contribution of the reduced burn durations and higher AHRR for LPG compared to CNG which was shown in Figure 2b. These differences between the fuels were linked to the superior laminar flame speed (LFS) shown in Table 3 and the fuel energy density [8] of LPG compared to CNG. The LFS was calculated at STP using the ALPINE_153 mechanism in CHEMKIN [55].

4.2. Effect of Engine Load

Engine load, represented by the net IMEP, was swept at CR 8:1 from 8bar until the load limit of the engine at 11bar was reached. The results for both fuels

are presented in this section. The in-cylinder pressures and AHRR for the LPG and CNG fueling configuration at 8bar and 11bar are shown in Figure 3a. The LPG pressure traces indicated higher peak in-cylinder pressures, 6.5% higher at 8bar engine load and 10% higher at 11bar, with LPP also closer to TDC than their CNG counterparts. Another feature of the in-cylinder pressure traces was the steeper slope observed for LPG as its rate of pressure rise differed markedly from that for CNG. Similar to the CR case in Section 4.1, LPG demonstrated faster AHRR with much higher peaks than CNG. For example, the peak AHRR at 11bar engine load was 0.24kJ/deg for LPG compared to 0.1kJ/deg for CNG. The shape of the AHRR curves, at 8bar engine load for LPG, with the distinctive shoulder also suggested the presence of a secondary combustion event typically associated with end-gas auto-ignition. These dissimilar combustion characteristics were due to the differences in reactivity of the primary constituents of both fuels, Propane for LPG, and Methane for CNG.

Figure 3b shows the knock integral (KI) characteristics of both fuels at the same engine operating conditions, CNG demonstrated a clear advantage owing to its ON/MN as previously discussed in Section 4.1, remaining below the knock limit at all engine loads. LPG on the other hand, started to experience light knock from 8bar engine load as was suggested by the distinctive shoulder on the AHRR curve. LPG also indicated an exponential rise in knocking intensities as engine load was increased. For both fuels, however, the KI increased with increasing engine load.

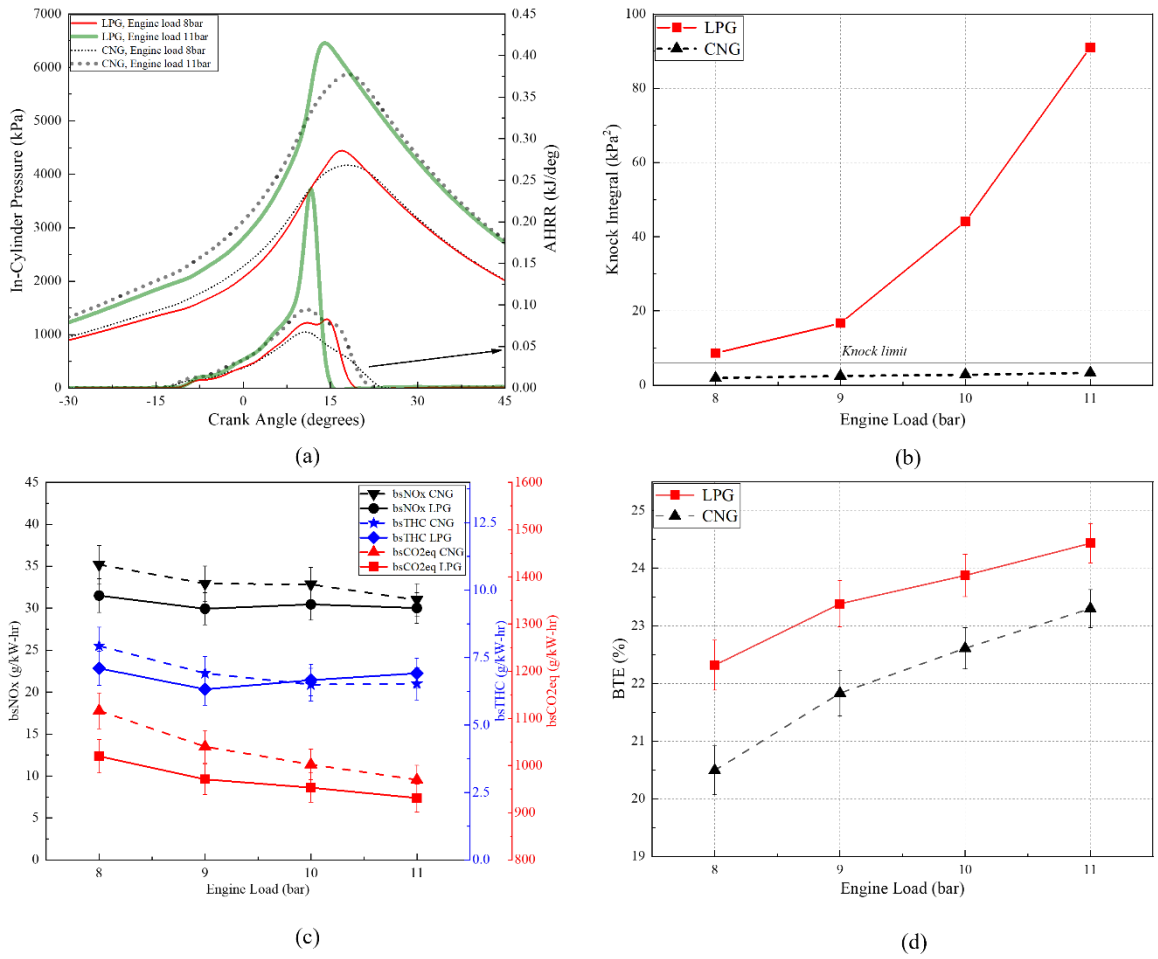

Figure 3: Variation of (a) In-cylinder pressure and AHRR (b) Knock Integral (c) brake specific emissions (d) BTE, with engine load for CNG and LPG

The brake specific NOx, THC and CO_2eq are shown in Figure 3c for both tested fuels. The bsNOx values for CNG were observed to be higher than for LPG at all engine loads. In addition to the in-cylinder temperature and brake power normalization discussions mentioned in Section 4.1, the N_2 present in the CNG fuel and quantified in Table 3 may be a possible contributor to the CNG NOx emissions. However, the normalization by a lower brake power remains

the key reason for the higher bsNOx emissions of CNG despite the higher ideal gas peak in-cylinder temperature of LPG compared to CNG (for example 2851K compared to 2744K at 8bar engine load) and its effect on the raw NOx ppm values. Figure 3c also illustrates the variation of the brake specific THC for both tested fuels across the engine loads. HC emissions are primarily due to the incomplete combustion of the fuel. From the results, CNG and LPG demonstrated opposing trends as load was increased; similar trends were also observed for CNG and LPG [59] and LPG only [34]. Finally, $bsCO_2eq$ emissions are shown in Figure 3c. These composite GHG emissions combine the effect of CO_2, CH_4 with a 25-unit multiplier, and N_2O with a 298 multiplier to present a CO_2 equivalent emissions metric. These emissions, although dominated by the $bsCO_2$ emissions, demonstrate the importance of considering the CH_4 and N_2O emissions. Due to its higher H:C ratio shown in Table 3, the $bsCO_2$ emissions of CNG at all tested engine loads were considerably lower than the LPG $bsCO_2$ similar to results presented in the literature [58]. Nevertheless, CNG produced significantly higher $bsCO_2eq$ emissions at all tested engine loads, showing a 10% increase at low engine loads and a 4% increase in $bsCO_2eq$ at the engine load limit compared to LPG. This trend is a result of the higher concentrations of CH_4 emissions, a potent GHG, produced by CNG.

BTE, shown in Figure 3d, increased as engine load was increased as a result of minimized friction and pumping losses at the boosted engine conditions [3, 11]. Comparing CNG and LPG BTE values, LPG produced a maximum BTE of

24.4% at the engine load limit, a 5% relative improvement in efficiency compared to CNG at the same engine load. The largest improvement was recorded at 8bar engine load where CNG produced a BTE of 20.5%, 9% relatively lower than the LPG BTE at this condition. The fuel effect on BTE was discussed in Section 4.1 with another possible contributor, captured in Figure 3a, being the proximity of the LPP to TDC with LPG combustion compared to CNG, which suggests increased work transfer to the piston.

4.3. Effect of Exhaust Gas Recirculation (EGR)

The results from the CR and engine load investigations were then analyzed and informed the EGR tests. This section presents the influence of EGR dilution on the performance, emission, and combustion behavior of both fuels. EGR was added to the fuel-air mixture at CR 8:1 and 9:1 with the engine load maintained at 10bar by varying the IMAP. Details of the combustion characteristics are presented in Figure 4. Figures 4a and 4b illustrate the interaction between the KI, the combustion stability expressed in terms of the $COV_{peak\ pressure}$, and the EGR rate. As EGR is added and the intake charge becomes more diluted and less reactive, the COV increases to a limit above which combustion can be said to be unstable, usually marked by high cycle-to-cycle variability. In this study, a $COV_{peak\ pressure}$ of 10% was adopted as the COV limit, and the EGR% at which this COV limit was reached referred to as the EGR limit.

Accordingly, as EGR% was increased in Figures 4a and 4b, the $COV_{peak\ pressure}$ also rose until it crossed the 10% limit for both CNG and LPG. LPG

indicated a higher tolerance for dilution with EGR, with an EGR limit of 26% at CR 8:1, achieving a 13% relative improvement compared to the EGR limit for CNG. At CR 9:1 the dilution tolerance gap was even wider as LPG indicated an EGR limit of 28%, achieving double the relative improvement (27%) compared to CNG. This improvement in EGR tolerance could likely be due to the differences in early flame development and flame propagation times linked to the superior flame speed of LPG shown in Table 3. For example, at CR 9:1 and 30% EGR, the 10-90% mass fraction burned duration was calculated to be 22.3 CAD for LPG and 34.8 CAD for CNG. However, recent computational studies by Ge et al. [52] comparing two fuels of similar flame speed still showed significant differences in EGR dilution tolerances and they proposed the Lewis number or low temperature chemistry as more dominant factors in EGR dilution mechanics. Therefore, these experimental results suggest that fuel low temperature chemistry may possibly be the key factor in determining EGR dilution tolerance as despite the lower Lewis number of CNG (~1 for Methane and ~1.8 for Propane [52]), LPG still demonstrated substantially improved EGR dilution tolerances. These effects were likely amplified by increasing the CR for LPG in particular, as it was discovered that the CNG EGR limit remained approximately the same at both CR.

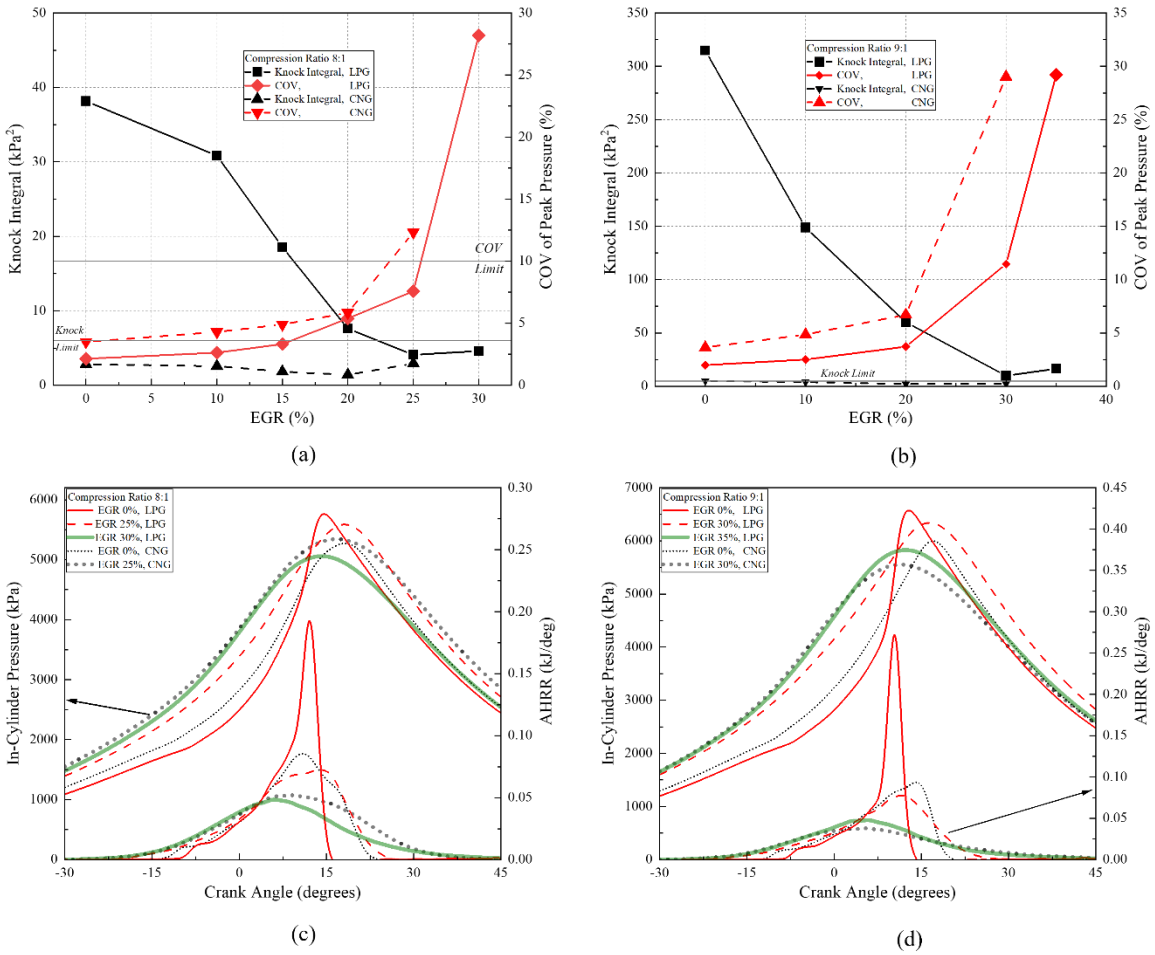

Figure 4: Various combustion metrics at different EGR rates for CNG and LPG and at different compression ratios: (a) Knock Integral and $COV_{peak\ pressure\ @CR8:1}$ (b) Knock Integral and $COV_{peak\ pressure\ @CR9:1}$ (c) In-cylinder pressures and AHRR $_{@CR8:1}$ and (d) In-cylinder pressures and AHRR $_{@CR9:1}$

A documented desired effect of EGR is its mitigating effect on knock, thus allowing engine operation at higher CR and engine loads especially for fuels with high reactivity such as LPG. This effect was demonstrated especially for LPG, in Figure 4a, as the KI was reduced by 84% from medium knock levels to

a stable, knock-free engine operation in the window between 22% EGR and the EGR limit at 26%. From Figure 4b, it is seen that the KI was reduced even more remarkably by 98% at the higher CR, as the engine was transitioned from heavy, destructive knock without EGR to light knock at the EGR limit. These effects were much less pronounced with CNG as the engine only experienced some level of incipient knock at CR 9:1 without EGR, and they were quickly counteracted by the increased dilution.

The in-cylinder pressure traces and AHRR at CR 8:1 and 9:1 are shown in Figures 4c and 4d. For LPG, the addition of EGR was observed to reduce the peak in-cylinder pressures and retard the LPP up until the EGR limit at both CR. In the case of CNG, a similar trend was observed at CR 9:1 with a slight difference at CR 8:1, where only the LPP trend was observed, and peak pressures remained approximately equal. The AHRR curves also described very definitive trends for both fuels. For LPG, the peak AHRR was reduced by 62% from 0.19kJ/deg without EGR to 0.07kJ/deg around the EGR limit at CR 8:1 and from 0.27kJ/deg without EGR to 0.08kJ/deg around the EGR limit at CR 9:1. For CNG, a similar peak AHRR reduction trend was observed but by lesser amounts: 38% at CR 8:1 and 60% at CR 9:1. A key feature of the AHRR curves for both fuels was the longer AHRR duration as EGR was introduced, indicating longer burn durations in the combustion chamber. Ravi et al. [40] showed similar combustion behaviors in their study.

In terms of brake specific emissions presented in Figures 5a and 5b, LPG

bsNOx was reduced by 80% from 32.24g/kW-hr to 6.7g/kW-hr as EGR was introduced to the intake charge from 0% up to the EGR limit at CR 8:1. This reduction was furthered at CR 9:1, as bsNOx was minimized by around 90% from 34g/kW-hr to 3.5g/kW-hr within the same EGR window, while the bsNOx was reduced by approximately 70% for CNG at both CR. This trend continued even after the EGR limit when combustion had become unstable. This EGR influence on NOx is a result of the elevated heat capacity of the cylinder charge due to introduction of exhaust gases, and the decreased flame temperatures, which effectively reduce NOx. This mitigating effect of EGR on NOx is outlined in the literature [12, 50, 40]. As combustion transitioned from slow burn w.r.t increasing EGR rates to misfire after the EGR limit, the bsTHC emissions remained fairly constant around 7g/kW-hr up until the EGR limit and then spiked to over 6 times that value to greater than 42g/kW-hr for both CNG and LPG at CR 9:1 suggesting misfire at those extremes. At CR 8:1, LPG bsTHC indicated similar trends to those exhibited at CR 9:1; however, while the bsTHC emissions for CNG increased after its EGR limit, it was not as dramatic as was observed for LPG. As discussed above, this EGR - bsTHC behavior resulted from decreased burn rates as combustion transitioned from slow burn to misfire, leading to the incomplete combustion of the fuel. These trends were also captured by Bayliff et al. [50].

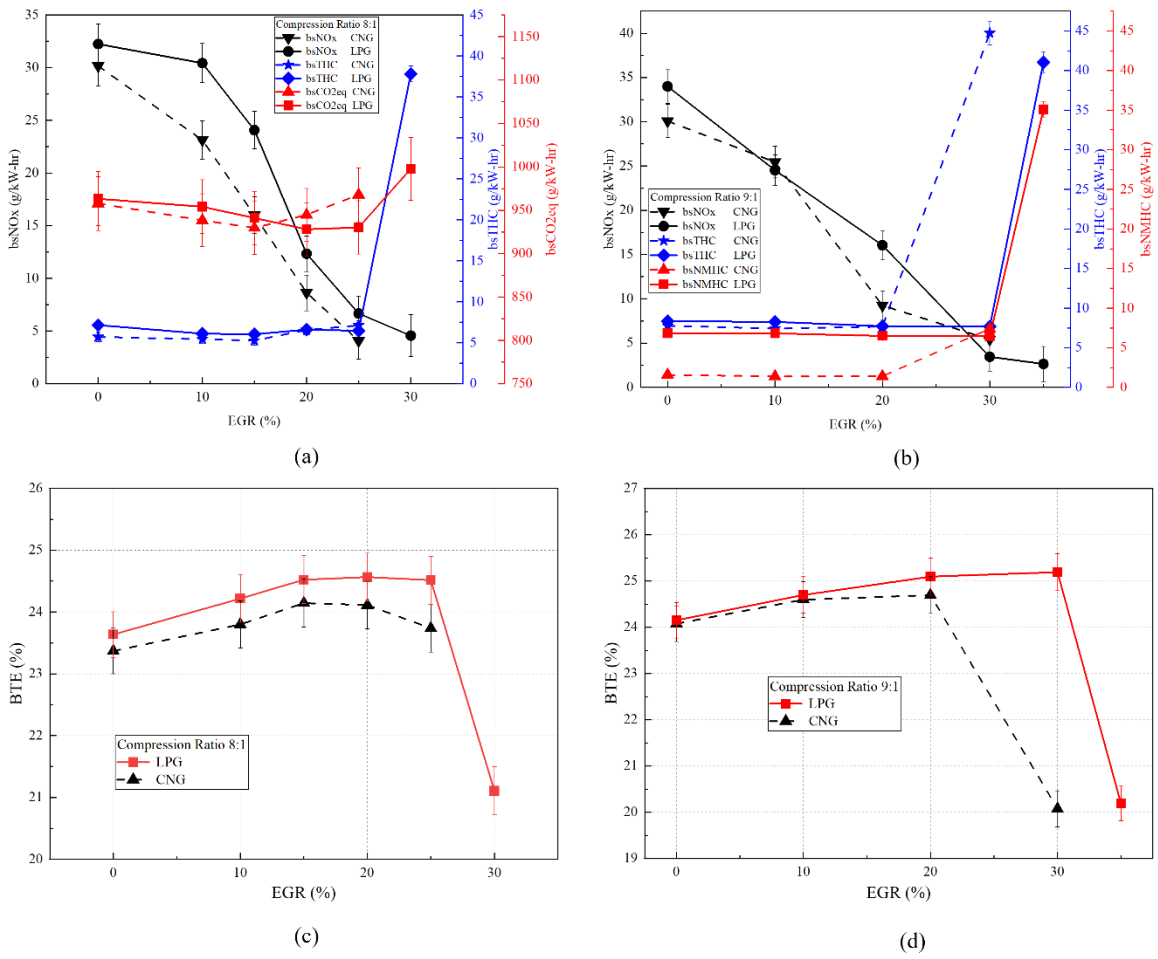

Figure 5: Plots of emission and performance metrics at various EGR rates for CNG and LPG and at different compression ratios showing (a) brake specific emissions $_{@CR8:1}$ (b) brake specific emissions $_{@CR9:1}$ (c) BTE $_{@CR8:1}$ and (d) BTE $_{@CR9:1}$

Finally, $bsCO_2eq$ emissions are shown for both fuels at CR 8:1 in Figure 5a while bsNMHC are shown for both fuels at CR 9:1 in Figure 5b. As discussed in Section 4.1, the bsNMHC for CNG was observed to be significantly lower compared to the bsNMHC of LPG, and this trend persisted as EGR rates were

increased. Although CNG was mainly Methane, the presence of NMHC in its exhaust emissions is due to the recombination reactions to higher hydrocarbons which can be found in the low temperature chemistry of Methane. There are also the 10% by vol C_2H_6 and 1.3% by vol C_3H_8 present in the fuel shown in Table 3 which can escape as unburnt hydrocarbons from the crevice volumes or during misfires/partial combustion. After the EGR limit, this bsNMHC produced by CNG rose to approximately match the bsNMHC at the EGR limit of LPG. In this regard, CNG had exceeded its EGR limit but still produced low enough bsNMHC at around 6.5g/kW-hr to match that of LPG even though LPG was still within its EGR limit. In Figure 5a, the bsCO_2eq emissions decreased with increased EGR, then began to rise a few percentages before the EGR limit for both fuels, suggesting that if all relevant emissions are considered, an optimal EGR amount may not necessarily exist at the EGR limit but slightly retarded from that EGR%.

Figures 5c and 5d present the BTE for both fuels at the two tested CR. BTE demonstrated an increasing trend up until the EGR limit for both fuels, this influence of EGR on BTE was likely a result of reduced pumping work and fuel consumption as well as reduced heat loss in the combustion chamber as temperatures were much lower [60]. For example, pumping work calculated from the in-cylinder pressure data was reduced by 11% from 98J at 0% EGR to 87J at the EGR limit for LPG at CR 8:1. After the EGR limit, however, BTE dropped sharply for both fuels due to the unstable combustion illustrated by the

high $COV_{peak\ pressures}$ associated with high dilutions shown in Figures 4a and 4b. These high $COV_{peak\ pressures}$ underscored misfire/partial combustion which was responsible for the elevated bsTHC emissions in Figures 5a and 5b which in turn would have a deleterious effect on combustion efficiency and BTE. Comparing the fuels, the disparity in performance was more obvious for all EGR rates at CR 8:1 with LPG fueling responsible for a maximum 3% relative improvement over CNG at 25% EGR. Conversely, the brake thermal efficiencies of the fuels were more closely matched at CR 9:1, until a strong divergence point at 30% EGR, where LPG achieved a 25% relative improvement in performance as a result of its higher EGR tolerance. The maximum BTE recorded during this study was 25.2%, achieved with LPG fueling at CR 9:1, 10bar engine load, and 30% EGR.

4.4. Combustion Intensity Metric (CIM)

Finally, this study explored the possible benefits on the combustion and performance of LPG using the real-time ignition timing control tool, the combustion intensity metric (CIM). The CIM, a robust combustion control tool, which takes into account several key combustion metrics outlined in equation 4 had been previously applied for natural gas operation optimization [45, 47 - 49]. The CIM which was used to initiate a desired fraction of end-gas auto-ignition (f-EGAI), was successfully recalibrated for use with LPG in this study. Figure 6a shows the relationship between CIM and f-EGAI for CNG and LPG. The CNG data, culled from previous work on the CFR engine by Bayliff et al. [50] described a steeper relationship, 0.15 to 0.53 f-EGAI as CIM was varied from 20

to 80%, compared to the narrower control region indicated for LPG, 0.31 to 0.5 f-EGAI. This was an indication that LPG transitioned more suddenly into end-gas auto-ignition as opposed to CNG, which exhibited a steadier climb into end-gas auto-ignition. The fuel reactivity and knock resistance, discussed in Sections 4.1 and 4.2, are likely responsible for this trend.

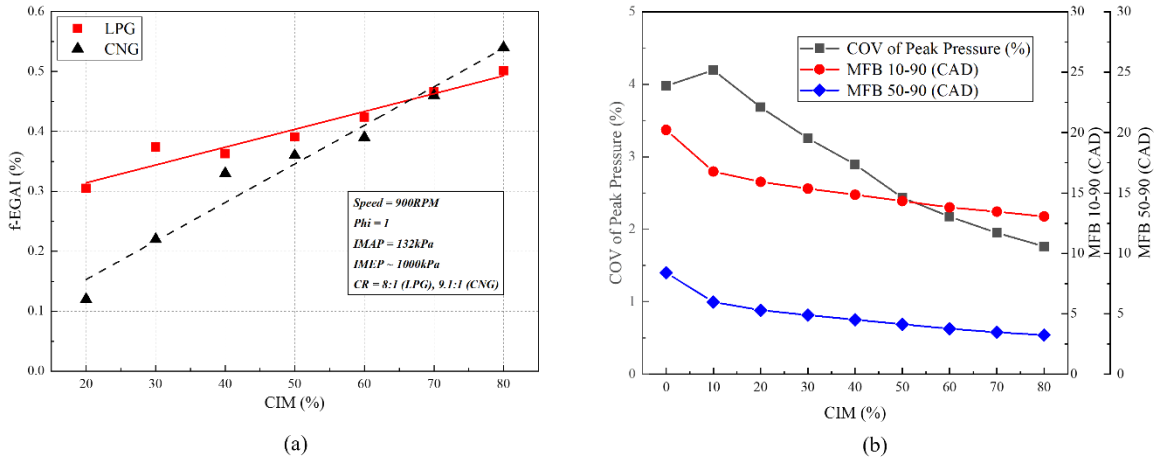

Figure 6: (a) fraction of end-gas auto-ignition vs CIM (b) $COV_{peak\ pressure}$, MFB 10-90% and MFB 50-90% vs CIM

In Figure 6b, the $COV_{peak\ pressure}$, MFB 10-90% and 50-90% are shown. Hampson et al. [45] suggested that CIM could be responsible for effecting a more controlled volumetric ignition as opposed to isolated harmful pockets of end-gas auto-ignition. They suggested that this could be achieved by shortening the combustion duration and especially, the 50-90% time during which end-gas auto-ignition is most likely to occur so that desirable auto-ignition is happening

volumetrically all through the combustion chamber at approximately the same time. The trends showed that as CIM was increased, the 10-90% burn duration for LPG was reduced; however, more desirable was the reduction in 50-90% time in CAD, which even exhibited a slightly quicker decline compared to the 10-90% burn duration. The $COV_{peak\ pressure}$ was also shown to improve as CIM was increased suggesting less cycle-to-cycle variability, possibly linked to this volumetric auto-ignition and the quicker burn durations. Finally, the influence of CIM on performance is captured in Figure 7. The BTE increased from 23.1% at CIM 0% to a maximum at CIM 20% which corresponded to an f-EGAI of 0.31. Bayliff et al. [50] reported a similar result for CNG, with the maximum BTE w.r.t CIM observed at an f-EGAI of 0.33. This increase in BTE was the result of the advanced ignition timings as CIM was increased, which shifted the LPP closer to the TDC and increased work transfer to the piston.

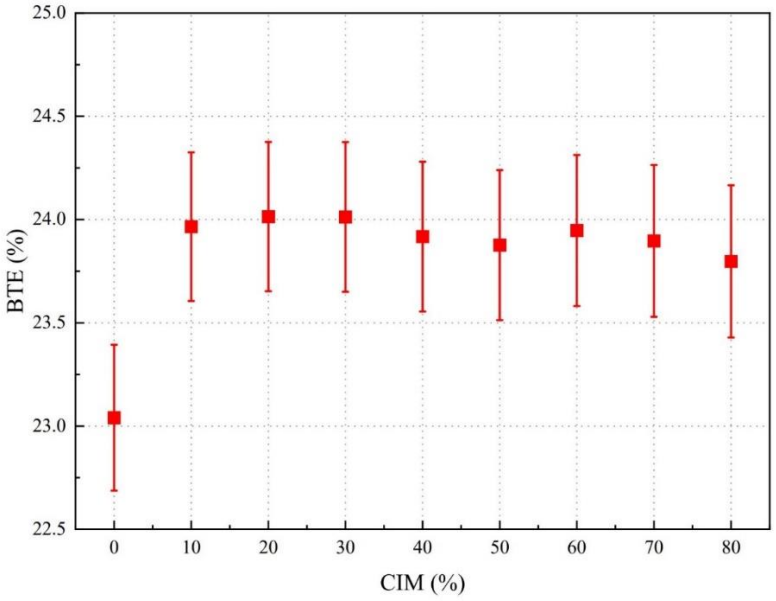

Figure 7: BTE vs CIM at ϕ = 1, CR = 8:1 and 10 bar engine load for LPG fueling

5. Conclusion

This study compared the combustion, emissions, and performance characteristics of two forefront low-carbon alternative fuels, LPG and CNG. Experimental investigations were conducted over a range of compression ratios, engine loads, and exhaust gas recirculation rates on a spark-ignited CFR engine. The application of a novel, robust combustion control tool was also explored for LPG after having previously been studied with CNG in different works. The main findings are summarized below:

- CNG demonstrated an advantage in terms of engine operation at higher engine loads and compression ratios, allowing knock-free engine operation up until the engine load limit and only experiencing medium level of knock at CR 12:1. On the other hand, LPG began to exhibit knocking combustion at lower compression ratios and engine loads and demonstrated a steeper rise in knock intensity as the engine transitioned into heavy knock at CR 10:1 and at the engine load limit. In general, however, LPG consistently indicated enhanced combustion characteristics with faster and higher AHRR, shorter burn durations, higher peak pressures, and closer to TDC locations of peak pressure compared to CNG.

- Despite the higher compression ratios achieved by CNG, LPG performed marginally better in terms of BTE, accounting for the highest BTE with 22.7% at CR 10:1 compared to 21.9% for CNG at CR 12:1. LPG also

performed significantly better at all tested engine loads, producing a maximum efficiency of 24.4% compared to 23.3% for CNG at the engine load limit.

- CNG was observed to generate significantly higher bsCO_2eq emissions, a direct consequence of its considerably higher CH_4 emissions despite indicating lower bsCO_2 emissions compared to LPG. For example, the CNG fuel was responsible for a 10% and 4% higher bsCO_2eq at low engine loads and at the engine load limit respectively.

- LPG indicated superior EGR tolerance compared to CNG at the two tested compression ratios with a maximum EGR limit of 28% at CR 9:1 compared to 22% for CNG at the same CR suggesting that fuel low-temperature chemistry had a more significant effect on EGR dilution tolerance than the Lewis number. This superiority was further demonstrated at the LPG EGR limits, as LPG accounted for a 3% relative improvement in BTE at CR 8:1 and a 25% relative improvement at CR 9:1.

- EGR demonstrated a strong effect on bsNOx reducing the engine-out bsNOx at CR 8:1 by 80% from 32.24g/kW-hr without EGR to 6.7g/kW-hr at the EGR limit and exhibiting an even stronger effect at CR 9:1 by eliminating 90% of the bsNOx within the same EGR window for LPG. Similarly, this effect was observed for CNG but to a lesser degree as

bsNOx was reduced by approximately 70% at both CR.

- EGR was found to be effective at mitigating heavy knock as it reduced the LPG knock intensity metric by 98% at CR 9:1, transitioning the engine from heavy knock without EGR to light knock at the EGR limit. For LPG at CR 8:1, this KI reduction was 84%. CNG, however, only began to experience incipient knock at CR 9:1, and as such, this EGR effect was not apparent.

- Finally, the combustion intensity metric (CIM) was successfully applied as a combustion control tool for LPG to perform controlled end-gas auto-ignition combustion and for performance enhancement. LPG operation demonstrated a 50% narrower region of control for the fraction of end-gas auto-ignition compared to CNG indicating a faster transition from normal combustion to an end-gas auto-ignition regime.

These findings suggest that the current work may perhaps be expanded in two directions for the future. First, to determine an optimal EGR rate considering efficiency and all relevant emissions and second, to apply the robust CIM tool to speed up the slower burn rates associated with higher EGR rates which may possibly extend the EGR limit and further increase efficiency.

Acknowledgements

This research was funded by U.S. Department of Energy's Office of Energy Efficiency and Renewable Energy (EERE) under the award number DE-EE0009198. The authors would like to thank the Colorado State University Energy Institute and its Powerhouse Energy Campus for providing the research facility and resources. Cummins Inc. and Argonne National Laboratory are also acknowledged as project partners.

References

[1] US Energy Information Administration, Monthly energy review - December 2022.

[2] World energy outlook 2021. International Energy Agency; 2021.

[3] Ağbulut U, Karagöz M, Sarıdemir S, Öztürk A. Impact of various metal-oxide based nanoparticles and biodiesel blends on the combustion, performance, emission, vibration, and noise characteristics of a CI engine. Fuel 2020;270:117521.

[4] Kalghatgi G, Levinsky H, Colket M. Future transportation fuels. Prog Energy Combust Sci 2018;69:103–5.

[5] Bae C, Kim J. Alternative fuels for internal combustion engines, Proc Combust Inst 2017;36:3389-413.

[6] Martins J, Brito F. Alternative fuels for internal combustion engines. Energies 2020;13(16):4086

[7] Demirbas A. Fuel properties of hydrogen, liquefied petroleum gas (LPG), and compressed natural gas (CNG) for transportation. Energy Sources 2002;24:601–10.

[8] Moussavi M, AI-Turk M. Compressed natural gas and liquefied petroleum gas as alternative fuels. J Energy Eng 1993;119:168–79.

[9] Kalghatgi GT. The outlook for fuels for internal combustion engines. Int J Engine Res 2014;15:383–98.

[10] Kalghatgi GT. Developments in internal combustion engines and implications for combustion science and future transport fuels. Proc Combust Inst 2015;35:101–15.

[11] Szybist JP, Busch S, McCormick RL, Pihl JA, Splitter DA, Ratcliff MA, Kolodziej CP, Storey JM, Moses-DeBusk M, Vuilleumier D, Sjöberg M, Sluder CS, Rockstroh T, Miles P. What fuel properties enable higher thermal efficiency in spark-ignited engines? Prog Energy Combust Sci 2021;82.

[12] Heywood JB. Internal combustion engine fundamentals. 2nd ed.. McGraw-Hill Education; 2018.

[13] Splitter D, Pawlowski A, Wagner R. A historical analysis of the co-evolution of gasoline octane number and spark-ignition engines. Front Mech Eng 2016;1.

[14] Malenshek M, Olsen DB. Methane number testing of alternative gaseous fuels. Fuel 2009;88:650–6.

[15] Fosudo T, Kar T, Marchese A, Windom B, Olsen D. The impact of LPG composition on performance, emissions, and combustion characteristics of a pre-mixed spark-ignited CFR engine. SAE technical papers, SAE

International;2022.

[16] Campbell M, Wyszyński LP, Stone R. Combustion of LPG in a spark-ignition engine. Source: SAE Trans 2004;113:628–37.

[17] Singh E, Morganti K, Dibble R. Dual-fuel operation of gasoline and natural gas in a turbocharged engine. Fuel (Guildford) 2019;237:694–706.

[18] Nutu NC, Pana C, Negurescu N, Cernat A, Mirica I. LPG as a fuel for diesel engines-experimental investigations. IOP Conf Ser: Mater Sci Eng 2017;252(1):12079.

[19] Elnajjar E, Selim MY, Hamdan MO. Experimental study of dual fuel engine performance using variable LPG composition and engine parameters. Energy Convers Manag 2013;76:32–42.

[20] Saleh HE. Effect of variation in LPG composition on emissions and performance in a dual fuel diesel engine. Fuel 2008;87:3031–9.

[21] Bestel D, Bayliff S, Xu H, Marchese A, Olsen D, Windom B. Investigation of the end-gas autoignition process in natural gas engines and evaluation of the methane number index. Proc Combust Inst 2021;38(4):5839–47.

[22] Mohr J. The effect of fuel reactivity and exhaust gas recirculation on knock propensity of natural gas (master's thesis), Colorado State University; 2020.

[23] Meyer R, Meyers D, Shahed SM, Duggal VK. Development of a heavy duty on-highway natural gas-fueled engine. SAE technical papers, SAE International;1992.

[24] Barroso PM, Ribas X, Pita M, Dominguez J, Seia ED. HD diesel engines development for alternative fuel use. SAE Int J Engines 2015;8:326–40.

[25] Mohammed K, Harry W. 4 L light duty LPG engine evaluated for heavy duty application. SAE Int J Fuels Lubr 2010;3:1–21.

[26] Fosudo T, Kar T, Windom B, Schlagel J, Olsen D. Performance, combustion and emissions evaluation of liquid phase port-injected LPG on a single cylinder heavy-duty spark ignited engine. SAE technical papers, SAE International; 2023.

[27] Pradeep Bhasker J, Porpatham E. LPG gaseous phase electronic port injection on performance, emission, and combustion characteristics of Lean Burn SI Engine. IOP Conf Ser: Earth Environ Sci 2016;40(1):12069.

[28] Darzi M, Johnson D, Ulishney C, Bade M, Zamani N. Baseline evaluation of ignition timing and compression ratio configurations on efficiency and combustion stability of a small-bore, two-stroke, natural gas engine. In: ASME international mechanical engineering congress and exposition, vol. 58417. American Society of Mechanical Engineers; 2017, V006T08A002.

[29] Boretti AA, Watson HC. Development of a direct injection high efficiency

liquid phase LPG spark ignition engine. SAE Int J Engines 2009;2(1):1639–49.

[30] Kar T, Fosudo T, Windom B, Olsen D, Hoke J, Rogers J. Development of a liquid-phase LPG delivery system for direct injection, spark-ignited engines. In: Internal combustion engine division fall technical conference, vol. 86540. American Society of Mechanical Engineers; 2022, V001T07A005

[31] Krieck M, Günther M, Pischinger S, Kramer U, Heinze T, Thewes M. Future specification of automotive LPG fuels for modern turbocharged DI SI engines with today's high pressure fuel pumps. SAE Int J Fuels Lubr 2016;9:575–92.

[32] Tuan NT, Dong NP. Theoretical and experimental study of an injector of LPG liquid phase injection system. Energy Sustain Dev 2021;63:103–12.

[33] Dube A, Vivekanand M, Ramesh A. Experimental studies on liquid phase LPG direct injection on a two-stroke SI engine. SAE Int J Engines 2019;12.

[34] Pradeep V, Bakshi S, Ramesh A. Direct injection of gaseous LPG in a two-stroke SI engine for improved performance. Appl Therm Eng 2015;89:738–47.

[35] Kalam M, Masjuki H. An experimental investigation of high performance

natural gas engine with direct injection. Energy (Oxford) 2011;36(5):3563–71.

[36] Fan B, Pan J, Yang W, Pan Z, Bani S, Chen W, He R. Combined effect of injection timing and injection angle on mixture formation and combustion process in a direct injection (DI) natural gas rotary engine. Energy 2017;128:519–30.

[37] Bestel D, Bayliff S, Marchese A, Olsen D, Windom B, Xu H. Multi-dimensional modeling of the CFR engine for the investigation of SI natural gas combustion and controlled end-gas autoignition. In: Internal combustion engine division fall technical conference, vol. 84034. American Society of Mechanical Engineers; 2020, V001T06A012.

[38] Bernardi Bestel D, Rodriguez J, Marchese A, Olsen D, Windom B. Detection and onset determination of end-gas autoignition on spark-ignited natural gas engines based on the apparent heat release rate. SAE technical papers, SAE International; 2022.

[39] Felipe Rodriguez J, Xu H, Hampson G, Windom B, Marchese A, B Olsen D. Heavy duty natural gas single cylinder research engine installation, commissioning, and baseline testing. Energy Power Eng 2022;14(06):217–32.

[40] Ravi K, Pradeep Bhasker J, Alexander J, Porpatham E. Influence of cooled exhaust gas recirculation on performance, emissions and

combustion characteristics of LPG fuelled lean burn SI engine. IOP Conf Ser: Mater Sci Eng 2017;263(6):62069.

[41] Kar T, Fosudo T, Slunecka C, Marchese A, Windom B, Olsen D. A study of propane combustion in a spark-ignited cooperative fuel research (CFR) engine. SAE technical papers, SAE International; 2022.

[42] Kar T, Fosudo T, Marchese A, Windom B, Olsen D. Effect of fuel composition and EGR on spark-ignited engine combustion with LPG fueling: Experimental and numerical investigation. Fuel (Guildford) 2022;327(C):125221.

[43] Krieck M, Günther M, Pischinger S, Kramer U, Thewes M. Effects of LPG fuel formulations on knock and pre-ignition behavior of a DI SI engine. SAE Int J Engines 2015;9:237–51.

[44] Morganti KJ, Brear MJ, Silva GD, Yang Y, Dryer FL. The autoignition of Liquefied Petroleum Gas (LPG) in spark-ignition engines. Proc Combust Inst 2015;35:2933–40.

[45] Hampson GJ. High efficiency natural gas engine combustion using controlled auto-ignition. In: Internal combustion engine division fall technical conference, vol. 59346. American Society of Mechanical Engineers; 2019, V001T03A019.

[46] Mohr J, Windom B, Olsen DB, Marchese AJ. Homogeneous ignition

delay, flame propagation rate and end-gas autoignition fraction measurements of natural gas and exhaust gas recirculation blends in a rapid compression machine. In: Internal combustion engine division fall technical conference, vol. 84034. American Society of Mechanical Engineers; 2020, V001T03A012.

[47] Nair S, Carlson J, Barta J, Hampson GJ. Performance comparison of vibration knock sensors and in-cylinder pressure for protection of gas and dual fuel engines. In: 10th dessau gas engine conference. 2017.

[48] Nair S, Hampson GJ, Carlson J. Controlled multi-staged combustion strategy for overcoming load limitations of fuel flexible gas / diesel engines. In: Meeting the future of combustion engines, CIMAC Congress, CIMAC world congress on combustion engine. 2019, p. 317.

[49] Bayliff S, Windom B, Marchese A, Hampson G, Carlson J, Chiera D, Olsen D. Controlled end gas auto ignition with exhaust gas recirculation on a stoichiometric, spark ignited, natural gas engine. In: Internal combustion engine division fall technical conference, vol. 84034. American Society of Mechanical Engineers; 2020, V001T03A011.

[50] Bayliff SM. Evaluation of controlled end gas auto ignition with exhaust gas recirculation in a stoichiometric, spark ignited, natural gas engine (master’s thesis), Colorado State University; 2020.

[51] Splitter D, Boronat V, Chuahy F, Storey J. Performance of direct injected

propane and gasoline in a high stroke-to-bore ratio SI engine: Pathways to diesel efficiency parity with ultra-low soot. Int J Engine Res 2021;22(12):3475–88.

[52] Ge W, Chuahy FD, Zhang P, Sankaran R, Splitter D, DelVescovo D, Lu T, Zhao P. A direct numerical simulation study of the dilution tolerance of propane combustion under spark-ignition engine conditions. Combust Flame 2023;247:112–495.

[53] Wise DM, Olsen DB, Kim M. Development of a lean burn methane number measurement technique for alternative gaseous fuel evaluation. In: Internal combustion engine division fall technical conference, vol. 56109. American Society of Mechanical Engineers; 2013, V002T02A014.

[54] Wheeler AJ, Ganji AR. Introduction to engineering experimentation. 3rd ed.. Upper Saddle River, N.J.: Pearson Higher Education; 2010.

[55] Slunecka C. Autoignition and flame speed of premixed liquefied petroleum gas in a rapid compression machine: Experimental results and reduced chemical kinetic mechanism (master's thesis), Colorado State University; 2023.

[56] BS EN 16726:2015+A1:2018: Gas infrastructure. Quality of gas. group H. 2018.

[57] Alternative fuels data center: Fuel properties comparison [online]. 2021,

[Accessed 12-Jun-2023].

[58] Bielaczyc P, Szczotka A, Woodburn J. A comparison of exhaust emissions from vehicles fuelled with petrol, LPG and CNG. IOP Conf Ser: Mater Sci Eng 2016;148(1):12060

[59] Selim MY, Radwan M, Saleh H. Improving the performance of dual fuel engines running on natural gas/LPG by using pilot fuel derived from jojoba seeds. Renew Energy 2008;33(6):1173–85.

[60] Kar T, Zhou Z, Brear M, Yang Y, Khosravi M, Lacey J. A comparative study of directly injected spark ignition engine combustion and energy transfer with natural gas, gasoline, and charge dilution. SAE Int J Fuels Lubr 2022;15:199–220

Nomenclature

AHRR - Apparent heat release rate

aTDC - After top dead center

bs - Brake specific

BTE - Brake thermal efficiency

c-EGAI - Controlled end-gas auto-ignition

CAD - Crank angle degrees

CFR - Cooperative fuel research

CIM - Combustion intensity metric

CNG - Compressed natural gas

CO - Carbon monoxide

CO_2 - Carbon dioxide

CO_2eq - Equivalent CO_2

COV - Coefficient of variation

CR - Compression ratio

DI - Direct injection

EGAI - End-gas auto-ignition

EGR - Exhaust gas recirculation

EVC - Exhaust valve closing

EVO - Exhaust valve opening

f-EGAI - Fraction of end-gas auto-ignition

FFT - Fast Fourier transforms

FTIR - Fourier transforms infrared

GHG - Greenhouse gases

HC - Hydrocarbons

IMAP - Intake manifold air pressure

IMEP - Indicated mean effective pressure

IVC - Intake valve closing

IVO - Intake valve closing

KI - Knock integral

Lambda (λ) - Excess air ratio

LECM - Large engine control module

LFS - Laminar flame speed

LHV - Lower heating value

LNG - Liquefied natural gas

LPG - Liquefied petroleum gas

LPP - Location of peak pressure

MN - Methane number

NMHC - Non-methane hydrocarbons

NOx - Nitrous oxides

ON - Octane number

PM - Particulate matter

ppm - parts per million

SI - Spark ignited

STP - Standard temperature and pressure

THC - Total hydrocarbons